European Journal of Pharmacology 853 (2019) 299–307

Contents lists available at ScienceDirect

European Journal of Pharmacology

journal homepage: www.elsevier.com/locate/ejphar

Full length article

Pharmacology of JNJ-28583113: A novel TRPM2 antagonist

Lawrence Fourgeaud[a,*], Curt Dvorak[a], Malika Faouzi[b], John Starkus[b], Sunil Sahdeo[a], Qi Wang[a], Brian Lord[a], Heather Coate[a], Natalie Taylor[a], Yingbo He[a], Ning Qin[a], Alan Wickenden[a], Nicholas Carruthers[a], Timothy W. Lovenberg[a], Reinhold Penner[b], Anindya Bhattacharya[a]

[a] Janssen Research & Development, LLC, 3210 Merryfield Row, San Diego, CA, 92121, USA
[b] Centre for Biomedical Research at the Queen's Medical Centre, Honolulu, HI, 96813, USA

ARTICLE INFO

Keywords:
TRPM2 antagonist
Oxidative stress
Cell death
Microglia
Cytokine

ABSTRACT

Transient receptor potential melastatin type 2 (TRPM2) is a cation channel activated by free intracellular ADP-ribose and reactive oxygen species. TRPM2 signaling has been linked to the pathophysiology of CNS disorders such as neuropathic pain, bipolar disorder and Alzheimer's disease. In this manuscript, we describe the discovery of JNJ-28583113, a potent brain penetrant TRPM2 antagonist. Ca^{2+} flux assays in cells overexpressing TRPM2 and electrophysiological recordings were used to test the pharmacology of JNJ-28583113. JNJ-28583113 was assayed *in vitro* on GSK-3 phosphorylation levels, cell death, cytokine release in microglia and unbiased morphological phenotypic analysis. Finally, we dosed animals to evaluate its pharmacokinetic properties. Our results showed that JNJ-28583113 is a potent (126 ± 0.5 nM) TRPM2 antagonist. Blocking TRPM2 caused phosphorylation of GSK3α and β subunits. JNJ-28583113 also protected cells from oxidative stress induced cell death as well as morphological changes induced by non-cytotoxic concentrations of H_2O_2. In addition, inhibiting TRPM2 blunted cytokine release in response to pro-inflammatory stimuli in microglia. Lastly, we showed that JNJ-28583113 was brain penetrant but not suitable for systemic dosing as it was rapidly metabolized *in vivo*. While the *in-vitro* pharmacology of JNJ-28583113 is the best in class, its *in-vivo* properties would need optimization to assist in further probing key roles of TRPM2 in CNS pathophysiology.

1. Introduction

TRPM2, also known as TRPC7 or LTRPC2, is the second member of the melastatin-related TRP channel subfamily. It is widely expressed in many tissues including brain, lung, liver, spleen, heart, and pancreas. TRPM2 forms a Ca^{2+}-permeable non-selective cation channel that is activated by intracellular adenosine diphosphate ribose (ADPR), a by-product of the oxidative stress pathway, and intracellular Ca^{2+}. (Faouzi and Penner, 2014; Hara et al., 2002; Perraud et al., 2003; Sumoza-Toledo and Penner, 2011). In addition, TRPM2 is indirectly activated during oxidative stress by reactive oxygen/nitrogen species triggering mitochondrial ADPR release as well as nuclear ADPR production through the PARP/PARG pathway (Perraud et al., 2005). Furthermore, TRPM2 is modulated by cytosolic factors such as calcium and calmodulin as well as changes in pH and temperature (Song et al., 2016; Starkus et al., 2007; Tan and McNaughton, 2016). TRPM2 activation leads to calcium entry and has been shown to contribute to cytokine production, insulin release, cell motility, oxidative stress, inflammation and cell death. (Knowles et al., 2013; Lange et al., 2009; Syed Mortadza et al., 2015; Takahashi et al., 2011; Yamamoto et al., 2008; Zhong et al., 2013). Recently, TRPM2 signaling has been shown to be essential in detecting excessive heat and plays a central role in antipyresis and cool seeking behaviors in response to noxious warm temperatures (Song et al., 2016; Tan and McNaughton, 2016).

Within the CNS, TRPM2 is mainly expressed by neurons and microglia and plays important roles in neuroinflammation, oxidative stress, ischemic reperfusion injury and neurodegeneration. In microglia, TRPM2 plays a key role in calcium signaling and responses to pathological concentration of ROS and zinc (Aminzadeh et al., 2018; Kraft et al., 2004; Miyanohara et al., 2018; Syed Mortadza et al., 2015). TRPM2 deficient microglia are protected from beta-Amyloid Peptide (1–42) (Aβ42) induced activation and displayed reduced TNF-α release (Alawieyah Syed Mortadza et al., 2018). TRPM2 also contributed to Aβ42 and reactive oxygen species induced toxicity in neurons (Fonfria et al., 2005; Li and Jiang, 2018). Genetically removing TRPM2 from the APP/PS1 animal model of Alzheimer's disease also suppressed microglia activation and reversed age-dependent spatial memory deficit (Ostapchenko et al., 2015). Genetic studies have also found an

* Corresponding author.
E-mail address: lfourgea@its.jnj.com (L. Fourgeaud).

https://doi.org/10.1016/j.ejphar.2019.03.043
Received 12 September 2018; Received in revised form 13 March 2019; Accepted 22 March 2019
Available online 06 April 2019

Table 1
IC50 comparison of known TRPM2 antagonists.

Name	IC50 at hTRPM2 (μM)	Assay Type	Reference
ACA	1.7	calcium flux	Kraft et al., 2006
FFA	70	electrophysiology	Hill et al., 2004a, Chen et al., 2012
3-MFA	76	electrophysiology	Chen et al., 2012
econazole	< 3	electrophysiology	Hill et al., 2004b
2-APB	1	electrophysiology	Togashi et al., 2008
7i	5.7	electrophysiology	Luo et al., 2018
Scalaradial	0.21	electrophysiology	Starkus et al. (2017)
2,3-dihydroquinazolin-4(1H)-one (D9)	3.7	electrophysiology	Zhang et al., 2018a

association between the TRPM2 gene and bipolar disorder (BD) (McQuillin et al., 2006; Xu et al., 2009). TRPM2 deficient mice displayed BD-related behavior (increased anxiety and decreased social responses) and increased glycogen synthase kinase-3 (GSK-3) phosphorylation, a key cellular target of Lithium. (Jang et al., 2015). A recent study has reported anti-depressant phenotype of TRPM2 knock out mice (Ko et al., 2019).

The pharmacology of TRPM2 antagonists are limiting, and in many ways, have hampered progress towards our understanding of TRPM2 biology. TRPM2 antagonists characterized to date (Table 1) have been very useful in characterizing TRPM2 currents in recombinant cells. However, their low potency, non-specificity and poor *in vivo* properties limit their use in systems physiology. Therefore, the development of TRPM2-specific antagonists remains necessary for better deciphering of TRPM2 functions as well as developing compounds with therapeutic potential.

2. Material and methods

2.1. Animals

Animal work described in this paper performed at Janssen was done in accordance with the Guide for the Care and Use of Laboratory Animals adopted by the US National Institutes of Health and the approval from Janssen Institutional Animal Care and Use Committee. Animals were acclimated for at least 5 days after receipt in the facility. They were socially housed in accordance with institutional standards, received food and water ad libitum and were maintained on a 12-h light/dark cycle.

2.2. 2.2. Cell culture

HEK293 cells stably expressing chimpanzee (chTRPM2-HEK) or rat (rTRPM2-HEK) TRPM2 were grown at 37 °C with 5% CO2 in Dulbecco's Modified Eagle's medium (DMEM) high glucose (Hyclone) supplemented with 10% fetal bovine serum (FBS) (Omega), Penicillin-Streptomycin (100 U/ml - Corning) and Geneticin (0.5 mg/ml - Gibco). HEK293 cells stably expressing human TRPM2 (hTRPM2-HEK) were grown at 37 °C with 5% CO2 in Modified Eagle's medium (MEM) (Corning) supplemented with 10% heat inactivated FBS (Gibco), L-Glutamine (2 mM - Hyclone), Penicillin-Streptomycin (100 U/ml – Corning) and Geneticin (0.5 mg/ml - Gibco). For patch-clamping experiments, inducible HEK293 human Flag-TRPM2-expressing cells (hTRPM2-HEK-inducible) were cultured at 37 °C with 5% CO2 in Dulbecco's Modified Eagle's medium (DMEM) supplemented with 10% FBS, blasticidin (5 μg/ml - Invitrogen) and zeocin (0.4 mg/ml - Invitrogen). For induction, hTRPM2-HEK cells were cultured in medium containing 1 μg/ml tetracycline (Invitrogen) 4h before recordings were performed. INS-1 and U937 cells were cultured at 37 °C with 5% CO2 in RPMI-1640 medium supplemented with 10% FBS. For patch-clamping experiments, cells were plated on coverslips coated with 100 μg/ml poly-L-lysine (Sigma) and allowed to settle for 30 min before experiments.

2.3. Immunocytochemistry

hTRPM2-HEK cells were fixed for 10 min in 4% paraformaldehyde (PFA)/4% sucrose in PBS, washed with PBS, incubated for 10 min in 100 mM glycine, permeabilized for 5 min in 0.2% Triton-X100 in PBS, washed with PBS, and nonspecific binding was then blocked by 40 min incubation in blocking buffer (2% IgG-free BSA in PBS). Cells were incubated for 1 h at room temperature with 2 μg/ml of anti-TRPM2 (Bethyl Laboratory A300-414A) diluted in blocking buffer, washed five times in PBS, and then incubated for 1 h at room temperature in the dark with Hoechst and 3 μg/ml of anti-Rabbit Alexa 488 coupled (Jackson ImmunoResearch Laboratories) diluted in blocking buffer. Coverslips were washed and mounted onto slides using Fluoromount-G (Southern Biotech). Images were acquired with a Zeiss LSM 700 confocal microscope using Plan-Apochromat 63X objective.

2.4. 2.4. FLIPR Ca^{2+} flux

18–24 h prior to the assay, cells were seeded at a density of 7500 cells/well onto poly-D-Lysine coated 384 well black walled clear bottom plates (Becton Dickinson). On the day of the experiment, cell plates were washed with assay buffer, containing (in mM): 130 NaCl, 2 KCl, 1 $CaCl_2$, 1 $MgCl_2$, 10 HEPES, 5 Glucose; pH 7.4. After the wash, cells were loaded with 2X Calcium-4 (Molecular Devices, Sunnyvale, CA, USA) dye solution in the assay buffer. JNJ-28583113 was prepared at 10 mM stock in DMSO. Cells were incubated with test compound and dye for 30 min. H_2O_2 (300 μM) was added online and real-time changes in fluorescence paralleling calcium influx were monitored using FLIPR Tetra® reader (Molecular Devices). Concentration response curves were constructed using peak calcium responses and are expressed as percent of control (defined as response to 0.3 mM H_2O_2 in vehicle).

2.5. 2.5. Patch-clamp recordings

hTRPM2-HEK-inducible cells were kept in sodium-based external Ringer's solution containing (mM): 140 NaCl, 1 CaCl2, 2 MgCl2, 2.8 KCl, 11 glucose, 10 HEPES-NaOH with a pH of 7.2 and osmolarity of 300 mOsmol. Intracellular pipette solutions contained (mM): 120 K-glutamate, 8 NaCl, 1 MgCl2, 10 HEPES-KOH. The internal Ca2 + concentration was buffered to 600 nM with 10 mM BAPTA and 7.25 mM CaCl2 (calculated with WebMaxC). TRPM2 currents were activated by adding 300 μM ADPR (Sigma) to the above pipette solution. The pH of the final solution was adjusted to pH 7.2 and osmolarity measured at 300 mOsmol. The pH of the final solution was adjusted to pH 7.2 and osmolarity measured at 300 mOsmol. Patch-clamp experiments were performed in the whole-cell configuration at 21–25 °C. Patch pipettes had resistances of 2–3 MΩ. Data were acquired with PatchMaster software controlling an EPC-9 amplifier. SmartSquirt delivery system (Auto-Mate Scientific) was used for rapid external solution application and exchanges. Voltage ramps of 50 ms spanning the voltage range from −100 to 100 mV were delivered from a holding potential of 0 mV at a rate of 0.5 Hz, typically over a period of 500 s. Voltages were corrected for a liquid junction potential of 10 mV. Currents were

filtered at 2.9 kHz and digitized at 100 μs intervals. Capacitive currents were determined and corrected before each voltage ramp. The development of currents for a given potential was extracted from individual ramp current records by measuring the current amplitudes at voltages of −80 mV and +80 mV. Data were analyzed with FitMaster (HEKA), and IgorPro (WaveMetrics).

2.6. Western-blot

hTRPM2-HEK cells were pretreated for 30 min with JNJ-28583113 followed by 10 min H_2O_2 (300 μM) treatment before being lysed on ice using N-Per lysis buffer (Thermo Fisher Scientific) supplemented with anti-protease and phosphatase cocktail (Thermo Fisher Scientific). Samples were run using 4–12% acrylamide gradient gels (Invitrogen) using MOPS buffer and transferred onto nitrocellulose membrane. Membrane were blotted using anti-TRPM2 (Bethyl Labs A300-413A), anti-phosphoGSK3β (Ser 9) (Cell Signaling clone D85E12), anti-GSK3β (Cell Signaling clone 3D10), anti-phosphoGSK3α (Ser21) (Cell Signaling clone 36E9) and anti-GSK3α (Cell Signaling clone D80D1).

2.7. High content image analysis

HeLa cells were seeded (2000 cells/well) onto black/clear 384-well PDL-coated imaging assay plates (Cell Carrier, PerkinElmer) in 90 μl of growth media and incubated for 24 h at 37°C. On day 2, 10 μl 10X JNJ-28583113 or DMSO control was added to cells at a final assay concentration of 1 μM and incubated at 37°C for 6 h 10 μM H_2O_2 was then added for 24h. After media removal, a mitochondrial dye (Mito Tracker Deep Red-FM) diluted in growth media was added to live cells for 30 min at 37°C, followed by fixation with 4% PFA and permeabilization with 0.3% Triton X-100 with PBS washes between each step. After blocking with 5% BSA, stains for endoplasmic reticulum (Concanavalin A, Alexa Fluor® 488 Conjugate), actin (Phalloidin Alexa Fluor® 555 Conjugate), and nucleus (Hoechst 33342, Trihydrochloride, Trihydrate) were added simultaneously. After final PBS washes, plates were sealed with foil. Cellular images were collected from plates using an Image Xpress high-content imaging reader (Molecular Devices). 400 morphological features were collected per image file using automated image analysis (Columbus, PerkinElmer) and phenotypic machine-learning classifications were performed using High-content Profiler analysis software (PerkinElmer).

2.8. Microglia isolation

Cortices from P0 to P2 C57BL/6 mouse pups (mixed gender) were dissected, stripped of meninges and mechanically dissociated with a hand homogenizer and a 25-gauge needle. The cell suspension was seeded into poly-L-lysine-coated (Sigma-Aldrich) T150 tissue culture flasks and maintained in DMEM/F12 (Gibco) with 10% FBS (Gibco) and 1% penicillin streptomycin (Corning) for 10–14 days to grow a confluent mixed astrocyte/microglia population. Cells were collected and applied to an antigen-antibody-mediated magnetic cell-sorting (MACS, Miltenyi Biotech) assay to positively select microglia. The mixed glial population was resuspended in MACS buffer (Miltenyi Biotech) and incubated with CD11b MicroBeads (Miltenyi Biotech). The cell suspension was then applied to LS separation column (Miltenyi Biotech) fitted into a QuadroMACS cell separator (Miltenyi Biotech). Unlabeled cells passed through the column while labeled cells remained captured in the magnetic field. After washing the column with MACS buffer, the column was then removed from the magnetic separator and flushed with MACS buffer to collect the purified microglia population. For an increased level of purity, the eluted microglia population was passed through a new LS separation column a second time.

2.9. **2.9. IL-1β ELISA**

JNJ-28583113 was added to microglia cells 1h before treatment with 10 ng/ml of LPS (Sigma-Aldrich) for 23h. Mouse IL-1β ELISA kit (R &D systems) was used for quantification of IL-1β in cell culture supernatants following the manufacturer's instruction.

2.10. **2.10. Cell Death Assay**

18–24 h prior to the assay, hTRMP2-HEK cells were plated at a density of 30 000 cells/well into poly-D-Lysine coated 96 well black walled clear bottom plates (Becton Dickinson). Following 1h incubation with JNJ-28583113, cells were treated with a range of concentration of H_2O_2 for 1 h. Cell death was quantified using Calcein AM Cell Viability Assay Kit (Trevigen) according to manufacturer's instruction.

2.11. BBB study

Six male Harlan Sprague Dawley Rats approximately 400 g in body weight were used. Animals received a bolus subcutaneous dose of 10 mg/kg JNJ-28583113 that was formulated at 5 mg/ml in 5% (v/v) 1-methyl-2-pyrrolidinone, 20% (v/v) Solutol HS 15, and 75% (v/v) water and was delivered in a volume of 2 ml/kg. Blood and tissue sampling were conducted at 0.5, 2, or 6 h post dosing. Blood and tissue samples were taken immediately after euthanasia by CO2 asphyxiation. Blood samples were placed in tubes containing K2 EDTA and placed on ice. Blood samples were centrifuged at 11000 g for 5 min then plasma was removed and stored at −80°C before analysis by LC/MS-MS. The brains from each animal were removed, frozen on powdered dry ice and stored at −80°C. The brain tissue was homogenized in 3 vol of water for determination of compound concentration in the brain by LC/MS-MS.

3. Results

To identify specific TRPM2 antagonists, we conducted a high throughput Ca^{2+} flux assay in human embryonic kidney cells (HEK293) stably overexpressing the chimpanzee TRPM2. We initiated calcium influx through TRPM2 channels by applying hydrogen peroxide (H_2O_2) which caused oxidative stress leading to TRPM2 activation via intracellular production of endogenous ADPR. As the ADPR binding site is located in the intracellular C-terminal region of the channel, this indirect means is the standard method for activating TRPM2 in intact cells. We monitored real time changes in fluorescence of a calcium-sensitive dye using the FLIPR Tetra® reader; 1 mM of H_2O_2 led to a fast rise in intracellular calcium that was absent in HEK293 parental cells that do not express TRPM2 (Fig. 1A). We screened the entire Janssen compound collection with this assay using 0.3 mM H_2O_2 and a substructure search of one of the hits led to the identification of the Ethyl {3-[4-(trifluoromethyl)phenyl]-5,6,7,8-tetrahydrocyclohepta[c]pyrazol-1(4H)-yl}acetate compound named JNJ-28583113 (Fig. 1B). This compound was potent with a half-maximal inhibitory concentration (IC_{50}) in nanomolar range in cells overexpressing chimpanzee (Fig. 1C and D) TRPM2 (IC_{50} = 100 ± 0.5 nM), rat (Fig. 1D) TRPM2 (IC_{50} = 25 ± 0.5 nM) or human (Fig. 1E) TRPM2 (IC_{50} = 126 ± 0.5 nM). JNJ-28583113 potency is very high compared with other known TRPM2 antagonist (Table 1). One caveat of our screen was the potential for false positives as compounds inhibiting the PARP or PARG enzymes that are responsible for ADPR production would behave like a TRPM2 antagonist (i.e. false positive). Therefore, we counter screened JNJ-28583113 at 10 μM in a PARP and PARG assay and it displayed no reactivity towards PARP or PARG (data not shown). To assess JNJ-28583113 cross reactivity against other known targets we tested it at 10 μM in an assay panel for multiple known kinases (Table 2), GPCRs and ion channels (Table 3). JNJ-28583113 showed no significant reactivity in any of those counter screens. Finally, we tested 10 μM JNJ-28583113 for antagonism against nine other TRP

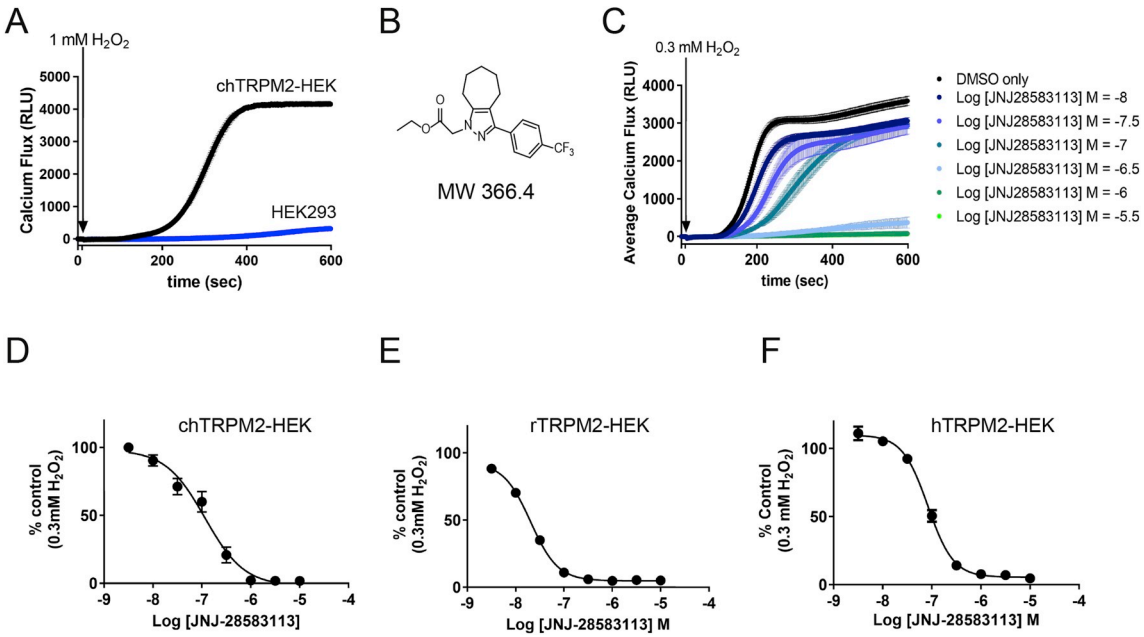

Fig. 1. JNJ-28583113 physical properties and pharmacological characterization in recombinant cells. (A) Example of average traces of Ca^{2+} FLIPR assay in chTRPM2-HEK and HEK293 cells in response to 1 mM H_2O_2. (B) Chemical structure and molecular weight of JNJ-28583113. (C) Example of average traces of Ca^{2+} FLIPR assay in chTRPM2-HEK pre-incubated with increasing concentration of JNJ-28583113 in response to 0.3 mM H_2O_2. (D) Ca^{2+} FLIPR assay antagonist concentration-response curve of JNJ-28583113 in chTRPM2-HEK cells in response to 0.3 mM H_2O_2. (E) Ca^{2+} FLIPR assay antagonist concentration-response curve of JNJ-28583113 in rTRPM2-HEK cells in response to 0.3 mM H_2O_2. (F) Ca^{2+} FLIPR assay antagonist concentration-response curve of JNJ-28583113 in hTRPM2-HEK cells in response to 0.3 mM H_2O_2. Data in D, E and F were constructed using peak calcium responses and are expressed as percent of control (defined as response to 0.3 mM H_2O_2 in vehicle). Symbols represent mean ± S.E.M. from 20 to 24 replicates performed in at least 2 independent experiments.

channels (TRPC3, TRPC5, TRPC6, TRPC7, TRPV1, TRPV4, TRPA1, TRPM5 and TRPM8) in a functional assay (plate-based fluorescence readout). The compound was clean at all TRP channels assayed except TRPM5 (Table 4).

To assess the effect of JNJ-28583113 directly on TRPM2 mediated currents, we performed patch-clamp experiments in HEK293 transiently overexpressing human TRPM2 (hTRPM2-HEK-inducible) (Fig. 2). TRPM2 currents were elicited by perfusing cells with ADPR through the patch pipette and buffering the intracellular free Ca^{2+} to 600 nM. ADPR is the physiological and primary direct trigger for activating TRPM2 channels thanks to the presence of NUDT9-H domain in the channel's C-terminal region. We and others have shown that intracellular calcium synergizes with ADPR to activate and sustain TRPM2 activity (McHugh et al., 2003; Starkus et al., 2007). Both ADPR and intracellular calcium concentrations were chosen to be optimal for both channel activation and current stabilization while being in the physiological range. We observed rapid and persistent activation of TRPM2 currents that were inhibited by extracellular application of increasing concentrations of JNJ-28583113 (Fig. 2A). The kinetics of block increased with drug concentration and we observed complete inhibition at or above 100 nM of JNJ-28583113. We measured the average inhibition as a function of drug concentration at 200 s of drug exposure (Fig. 2C) and JNJ-28583113 displayed an IC_{50} of 13 ± 2.8 nM. Current-voltage relationships of currents evoked by voltage ramps spanning −100 to 100 mV showed that TRPM2 inhibition was voltage independent and affected both inward and outward currents identically (Fig. 2B). The inhibitory effect of 1 μM JNJ-28583113 was mostly reversible and could be washed out relatively quickly (Fig. 2D). These results demonstrated that JNJ-28583113 is a potent and reversible TRPM2 antagonist.

Next, we used JNJ-28583113 to assess TRPM2 mediated signaling in multiple *in vitro* assays. TRPM2 activation was shown to inhibit glycogen synthase kinase-3 β (GSK-3β) and GSK-3α phosphorylation in Neuro2A cells in response to H_2O_2 (Jang et al., 2015). To see if JNJ-28583113 could affect this phenotype, we treated hTRPM2-HEK cells (Fig. 3A) with 300 μM H_2O_2 for 30 min and observed a robust decrease in GSK-3β phosphorylation levels by western blot that was fully prevented by 10 μM of JNJ-28583113 (Fig. 3B). We observed a similar decrease in GSK-3α phosphorylation level that was prevented by JNJ-28583113 in a concentration dependent manner (Fig. 3C). TRPM2 activation has also been linked to reactive oxygen species induced cell death in various cell types (e.g. U937, THP1, primary macrophages, primary microglia) (Hara et al., 2002; Zhang et al., 2003). To test if JNJ-28583113 could be protective in that context, we measured cell viability in hTRPM2-HEK cells in response to increasing concentration of H_2O_2. Pre-treatment with 10 μM of JNJ-28583113 prevented cells from H_2O_2 induced cell death up to 1 mM of H_2O_2 (Fig. 3D). This protective effect is maintained at 3 μM of JNJ-28583113 but is lost at 1 μM (Fig. 3E).

The next step was to assess the antagonism of JNJ-28583113 in native cells. Hence, we explored effects of JNJ-28583113 with subthreshold non-cytotoxic concentrations of H_2O_2 in HeLa and primary microglia cells. Using an unbiased highly sensitive multi-parametric high-content imaging assay, we measured subtle unbiased morphological phenotypic changes in response to low concentrations of H_2O_2 in HeLa cells that endogenously express TRPM2 (Gustafsdottir et al., 2013; Li et al., 2016). Cells were immuno-stained with multiple organelle markers (mitochondria, endoplasmic reticulum (ER), actin, nucleus) and analyzed by high-throughput microscopy (Fig. 4A). Greater than 400 morphological features were collected per cell using automated image analysis and machine-learning software to develop morphological classifications. 24h treatment with a low concentration (10 μM) of H_2O_2 consistently decreased the classification score reflecting specific morphological changes that occur in response to oxidative stress (Fig. 4A). Such morphological changes were prevented by pre-treatment 1 μM JNJ-28583113, indicating the phenotype induced by H_2O_2 was inhibited. These subthreshold concentrations of H_2O_2 did not decrease the number of cells after 24h (data not shown). Also, JNJ-28583113 did not prevent changes caused by inducers of ER stress (thapsigargin or tunicamycin) and mitochondrial stress (rotenone),

Table 2
JNJ-28583113 profiling in kinase assay panel.

Kinase Assay	Average activity (% control) in 10 μM of JNJ-28583113 (n = 2)
Abl(h)	104
Abl(m)	101
ACK1(h)	95
ALK4(h)	116
AMPKα1(h)	94
ASK1(h)	102
BrSK2(h)	108
CaMKIV(h)	99
CDK1/cyclinB(h)	98
CDK2/cyclinE(h)	110
CDK3/cyclinE(h)	94
CDK5/p25(h)	103
CDK9/cyclin T1(h)	106
CHK2(R145W)(h)	104
CLK2(h)	104
CLK3(h)	101
CLK4(h)	118
cKit(D816V)(h)	108
cSRC(h)	98
DRAK1(h)	94
EGFR(L858R)(h)	103
EGFR(L861Q)(h)	100
EphB3(h)	91
Fgr(h)	91
Flt4(h)	80
GRK1(h)	94
HIPK1(h)	98
IGF-1R(h)	119
IKKε(h)	94
IR(h)	106
IRAK1(h)	93
IRAK4(h)	92
JAK2(h)	118
KDR(h)	89
Lck(h) activated	110
LIMK1(h)	95
LKB1(h)	93
LOK(h)	100
Lyn(h)	110
Met(Y1248H)(h)	114
MKK6(h)	108
Mnk2(h)	96
MRCKβ(h)	102
mTOR/FKBP12(h)	110
MuSK(h)	82
NLK(h)	99
PAK2(h)	117
PAK5(h)	108
Pim-1(h)	116
PKA(h)	105
PKCζ(h)	100
PKD2(h)	104
PRAK(h)	75
PRK2(h)	110
ROCK-II(h)	117
Ron(h)	84
Rse(h)	107
Rsk1(h)	120
SGK(h)	110
SGK2(h)	103
STK33(h)	97
Tie2(Y897S)(h)	95
TLK1(h)	85
PI3 Kinase (p120g)(h)	93
PI3 Kinase (p110a(E545K)/p85a)(m)	99
PI3 Kinase (p110a(H1047R)/p85a)(m)	99
PI3 Kinase (p110d/p85a)(m)	99
PI3 Kinase (p110a(E542K)/p85a)(m)	101
PI3 Kinase (p110a(E542K)/p85a)(h)	95
PIP5K1a(h)	98

Kinase activity was assessed using Kinase Profiler™ assay (Eurofins).

Table 3
JNJ-28583113 profiling in GPCRs and ion channels assay panel.

Assays Tested	% inhibition in 10 μM of JNJ-28583113 (n = 2)
A1 (h) (antagonist radioligand)	< 10
A2A (h) (agonist radioligand)	< 10
A3 (h) (agonist radioligand)	30
alpha 1 (non-selective) (antagonist radioligand)	< 10
alpha 2 (non-selective) (antagonist radioligand)	10
beta 1 (h) (agonist radioligand)	< 10
AT1 (h) (antagonist radioligand)	< 10
BZD (central) (agonist radioligand)	< 10
B2 (h) (agonist radioligand)	< 10
CCK1 (CCKA) (h) (agonist radioligand)	22
D1 (h) (antagonist radioligand)	32
D2S (h) (antagonist radioligand)	< 10
ETA (h) (agonist radioligand)	< 10
GABA (non-selective) (agonist radioligand)	< 10
GAL2 (h) (agonist radioligand)	< 10
CXCR2 (IL-8B) (h) (agonist radioligand)	< 10
CCR1 (h) (agonist radioligand)	< 10
H1 (h) (antagonist radioligand)	< 10
H2 (h) (antagonist radioligand)	< 10
MC4 (h) (agonist radioligand)	< 10
MT1 (ML1A) (h) (agonist radioligand)	28
M1 (h) (antagonist radioligand)	< 10
M2 (h) (antagonist radioligand)	< 10
M3 (h) (antagonist radioligand)	< 10
NK2 (h) (agonist radioligand)	< 10
NK3 (h) (antagonist radioligand)	< 10
Y1 (h) (agonist radioligand)	< 10
Y2 (h) (agonist radioligand)	< 10
NTS1 (NT1) (h) (agonist radioligand)	< 10
delta 2 (DOP) (h) (agonist radioligand)	13
kappa (KOP) (agonist radioligand)	< 10
mu (MOP) (h) (agonist radioligand)	< 10
NOP (ORL1) (h) (agonist radioligand)	< 10
5-HT1A (h) (agonist radioligand)	< 10
5-HT1B (antagonist radioligand)	< 10
5-HT2A (h) (antagonist radioligand)	< 10
5-HT2B (h) (agonist radioligand)	32
5-HT3 (h) (antagonist radioligand)	< 10
5-HT5a (h) (agonist radioligand)	< 10
5-HT6 (h) (agonist radioligand)	< 10
5-HT7 (h) (agonist radioligand)	< 10
sst (non-selective) (agonist radioligand)	< 10
VPAC1 (VIP1) (h) (agonist radioligand)	< 10
V1a (h) (agonist radioligand)	12
Ca2+ channel (L, verapamil site) (phenylalkylamine) (antagonist radioligand)	< 10
KV channel (antagonist radioligand)	< 10
SKCa channel (antagonist radioligand)	< 10
Na + channel (site 2) (antagonist radioligand)	15
Cl- channel (GABA-gated) (antagonist radioligand)	26
norepinephrine transporter (h) (antagonist radioligand)	13
dopamine transporter (h) (antagonist radioligand)	12
5-HT transporter (h) (antagonist radioligand)	< 10

Activity was assessed by radio ligand binding (Eurofins). Values of ≤ 50% inhibition are non-significant in this assay.

demonstrating specificity for H_2O_2 induced reactive oxygen species (data not shown) (Kaufman, 1999; Li et al., 2003). TRPM2 activation has also been involved in chemokine and cytokine release in response to inflammation in multiple immune cell types (U937, THP1, monocytes) (Wehrhahn et al., 2010; Yamamoto et al., 2008). Therefore, we tested the effect of JNJ-28583113 on mouse primary microglia in culture by measuring IL-1β release. 24 h treatment with 10 ng/ml of lipopolysaccharide (LPS) led to increased IL-1β release which is significantly blunted by 10 μM JNJ-28583113 while lower concentration of the compounds had no significant effects (Fig. 4B). Together, our results showed that JNJ-28583113 is a potent tool to assess TRPM2 involvement across species and cell types *in vitro*.

Finally, to test for potential use of JNJ-28583113 as a therapeutic

Table 4
JNJ-28583113 profiling in calcium permeable TRP channels assay panel.

Assay Tested	10 μM of JNJ-28583113 Agonist mode	10 μM of JNJ-28583113 Antagonist mode
TRPC3	No effect	IC50 > 10 μM
TRPC5	No effect	No effect
TRPC6	No effect	IC50 > 10 μM
TRPC7	No effect	No effect
TRPA1	No effect	No effect
TRPM5	No effect	IC_{50} < 1 μM
TRPM8	No effect	No effect
TRPV1	No effect	No effect
TRPV4	No effect	enhancing effect

The cell lines were analyzed for the response to various compounds using a fluorescent Ca2+ sensitive dye, or a luminescence Ca2+ sensitive photoprotein or a membrane potential sensitive dye as readout. (Axxam).

compound, we assessed its blood brain barrier (BBB) permeability in rats. After subcutaneous (SC) injection (10 mg/kg), we detected JNJ-28583113 in the brain compartment at up to 400 ng/ml after 30 min (~1.1 μM estimated concentration) (Fig. 5A). However, we could not detect any measurable amount of JNJ-28583113 in the plasma. Since JNJ-28583113 was present in the brain, our results suggested that JNJ-28583113 was well distributed but highly unstable in the plasma. As JNJ-28583113 is an ester (see compound structure) and esterases are very active in the plasma, we hypothesized that JNJ-28583113 was hydrolyzed into its acid metabolite (Rudakova et al., 2011). We therefore tested for the presence of JNJ-28583113 acid metabolite in the same samples. We named the acid metabolite JNJ-61377069. As predicted we could detect high levels of JNJ-61377069 in plasma and low levels in the brain confirming that JNJ-28583113 was quickly metabolized in the plasma (Fig. 5B). We tested the potency of JNJ-61377069 in our Ca^{2+} FLIPR screening assay using chTRPM2-HEK cells and showed that this compound was totally inactive in blocking TRPM2 (IC50 > 10 μM). Such pharmacokinetic properties rendered JNJ-28583113 unsuitable for further development as an ideal tool compound for robust *in-vivo* pharmacokinetic-pharmacodynamic properties.

4. Discussion

In this study, we described JNJ-28583113, a potent reversible TRPM2 antagonist. JNJ-28583113 was identified from a substructure search of one of the hits obtained from a screen performed using a high throughput Ca^{2+} flux assay where TRPM2 was indirectly activated by ADPR production upon H_2O_2 application. Such an assay could lead to potentially identifying off target compounds, such as PARP and PARG inhibitors; in fact, we have found many such compounds in our screen. In addition to testing activity at PARP and PARG, it was also critical to use electrophysiological patch clamp recordings where TRPM2 was directly activated by intracellular application of ADPR to assess JNJ-28583113 potency. Our results confirmed that JNJ-28583113 was directly inhibiting human TRPM2 in a concentration-dependent manner in both recombinant and endogenous systems. From our pharmacokinetic studies, we also observed that JNJ-28583113 was brain penetrant but rapidly cleaved in the plasma leading to very transient exposure to the brain. Therefore, JNJ-28583113 is not an ideal *in vivo* tool compound candidate for chronic experimental conditions. Nonetheless, the transient brain exposure of JNJ-28583113 may be a good starter to address the role of TRPM2 in the CNS in the context of an acute drug challenge experiment.

With an IC_{50} of 126 nM for hTRPM2, JNJ-28583113 is potent compared to the most recently identified TRPM2 antagonists. For example, Scalaradial displayed an IC_{50} of 210 nM for hTRPM2, while the most potent of the 2,3-dihydroquinazolin-4(1H)-one derivates (D9) showed an IC_{50} of 3.7 μM for hTRPM2 (Starkus et al., 2017; Zhang et al., 2018a). Although JNJ-28583113 is potent in assays directly looking at TRPM2 functions (i.e. Ca^{2+} flux and electrophysiology (Figs. 1 and 2)), we observed a right shift in the efficacy of the compound when looking at the consequences of activating TRPM2 (i.e. cell death and cytokine release (Figs. 3 and 4)). This is a common observation when comparing direct versus secondary phenotypes involving many more steps to occur after channel activation. It is plausible that optimizing the concentrations of LPS (for IL-1b release) or H_2O_2 (for cell death) could titrate down the potency close to the ones found by measuring Ca^{2+} flux in FLIPR. However, from a drug discovery perspective, it is more important to generate a pharmacological effect such as shown here and focus medicinal chemistry efforts on future

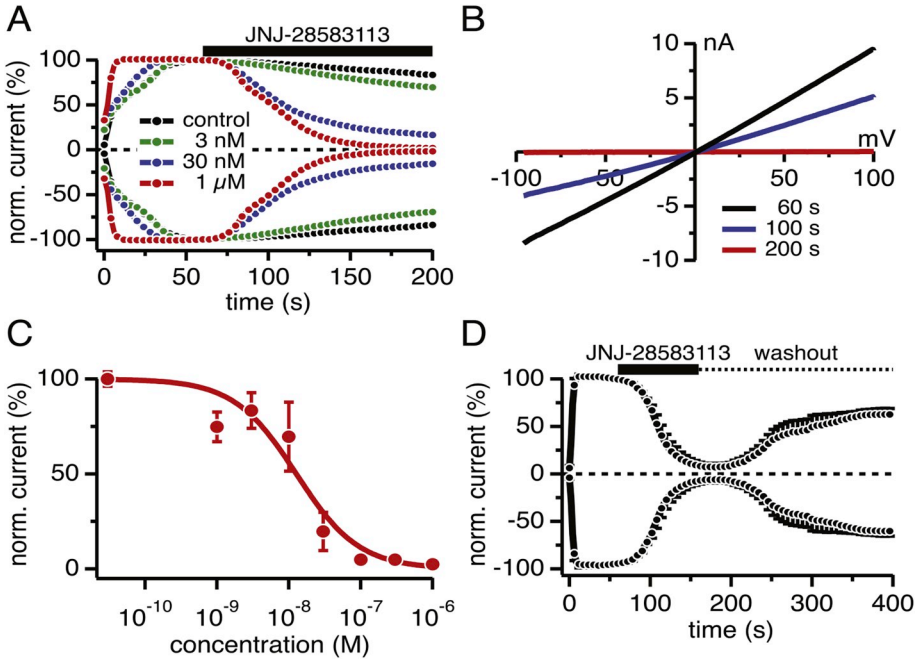

Fig. 2. Electrophysical characterization of JNJ-28583113 in ADPR-induced currents recorded in hTRPM2-HEK-inducible cells (A) Time course of average current amplitudes derived from currents evoked by voltage ramps and measured at +80 and −80 mV. Currents were normalized to amplitudes measured at 60 s just before extracellular application of various concentrations of JNJ-28583113 (3 nM, n = 12; 30 nM, n = 12; 1 μM, n = 8) or extracellular solution (control, n = 9). (B) High-resolution TRPM2 currents evoked by 50 ms voltage ramps from −100 mV to 100 mV from a holding potential of 0 mV, demonstrating a linear current-voltage (I–V) relationship with reversal of 0 mV. Data were obtained from an exemplary cell prior to (60 s), during (100 s) and at the end of 1 μM JNJ-28583113 application (200 s). (C) Concentration-response curve fit to mean normalized current amplitudes ± S.E.M. (n = 4–12), obtained at 80 mV and at 200 s (IC50 = 13 ± 2.8 nM). (D) Time course of average current amplitudes derived from currents evoked by voltage ramps and measured at 80 and -80 mV. Currents were normalized to amplitudes measured at 60 s just before extracellular application of 1 μM JNJ-2853113 (n = 4). After 100 s of application the drug was washed out with drug-free external saline to assess reversibility of block. Round symbols represent normalized averaged current amplitudes.

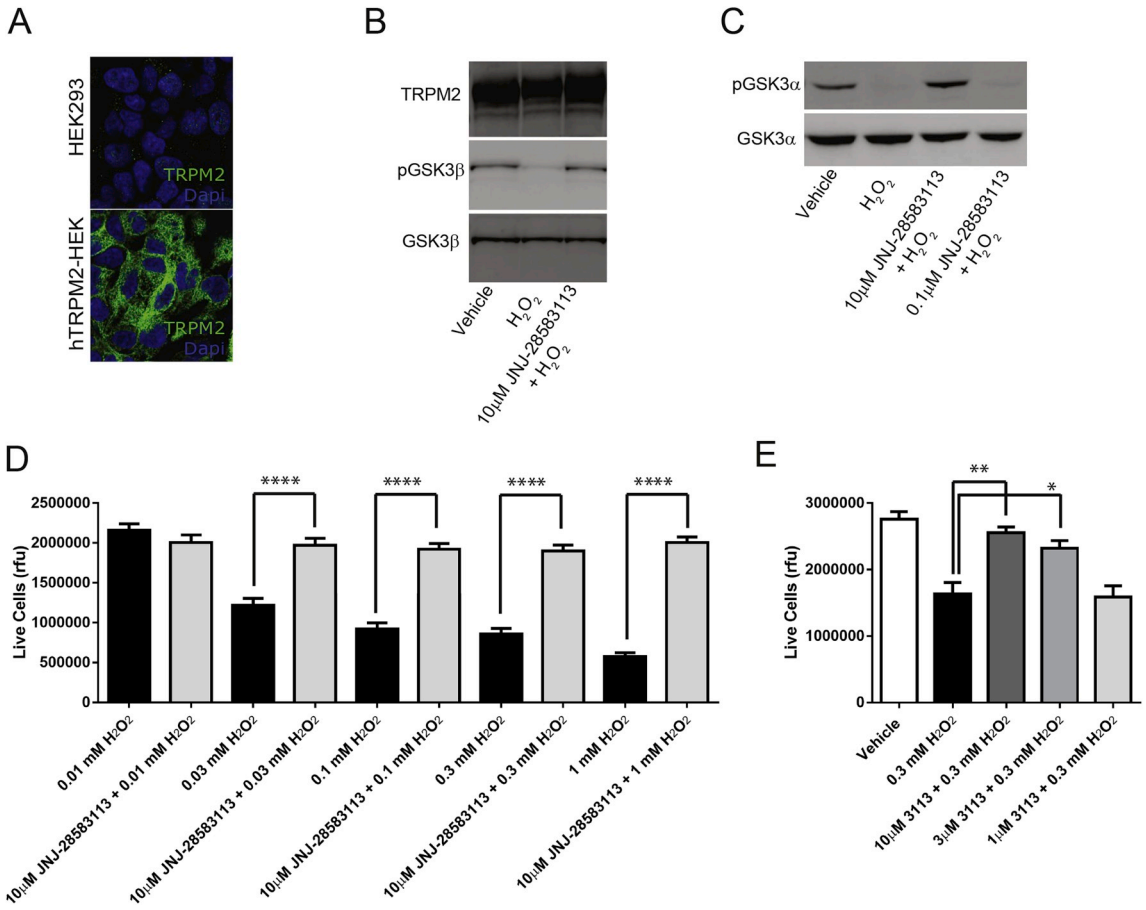

Fig. 3. In vitro engagement assays in hTRPM2-HEK cells. (A) Representative TRPM2 immunostaining in HEK293 and hTRPM2-HEK cells (B) Representative western blot of hTRPM2-HEK cell lysates showing that 10 min of H_2O_2 (300 μM) treatment led to a de-phosphorylation of GSK3β that is prevented by JNJ-28583113 (10 μM). (C) Representative western blot of hTRPM2-HEK cell lysates showing 10 min of H_2O_2 (300 μM) treatment led to a de-phosphorylation of GSK3α that is prevented by JNJ-28583113 in a concentration dependent manner. (D) and (E) Average data from Calcein-AM cell death assay performed in hTRPM2-HEK cells showing that JNJ-28583113 protects from H_2O_2 induced cell death. Bar graphs represents mean ± S.E.M. from at least 12 experimental replicates from 3 independent experiments. ****P < 0.0001, ***P < 0.001 and *P < 0.01 with ANOVA followed by Sidak's multiple comparison test.

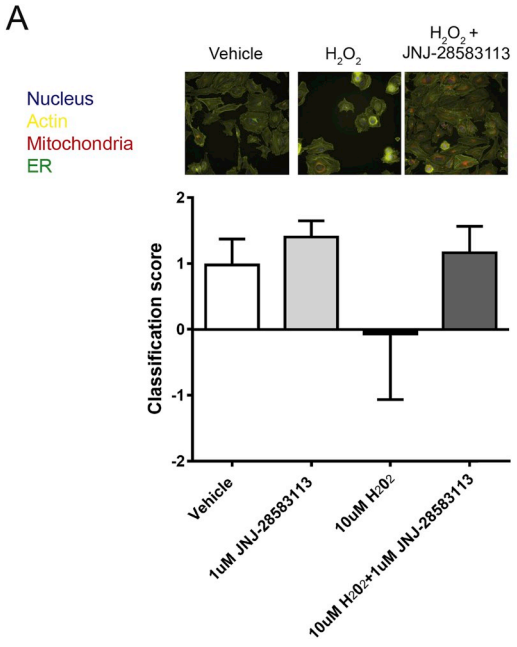

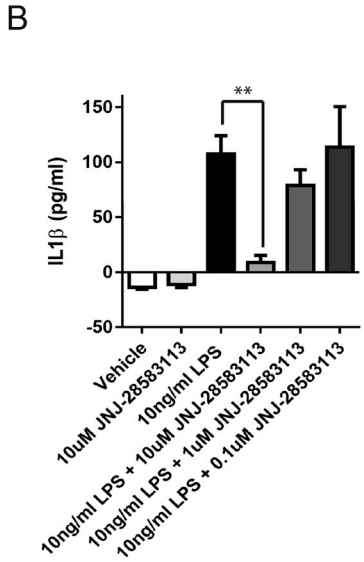

Fig. 4. In vitro engagement assays in native cells (A) Representative immunostaining of HeLa cells with all the markers used for high content image analysis. Average bar graph of classification score normalized to vehicle showing that JNJ-28583113 protects HeLa cells from H_2O_2 (10 μM) induced morphological changes. (B) Average data of IL-1β release amounts measured by ELISA showing that JNJ-28583113 inhibits IL-1β release in response to LPS in mouse primary microglia. Bar graph represent mean ± S.E.M. from 2 independent experiments. **P < 0.01 with ANOVA followed by Sidak's multiple comparison test.

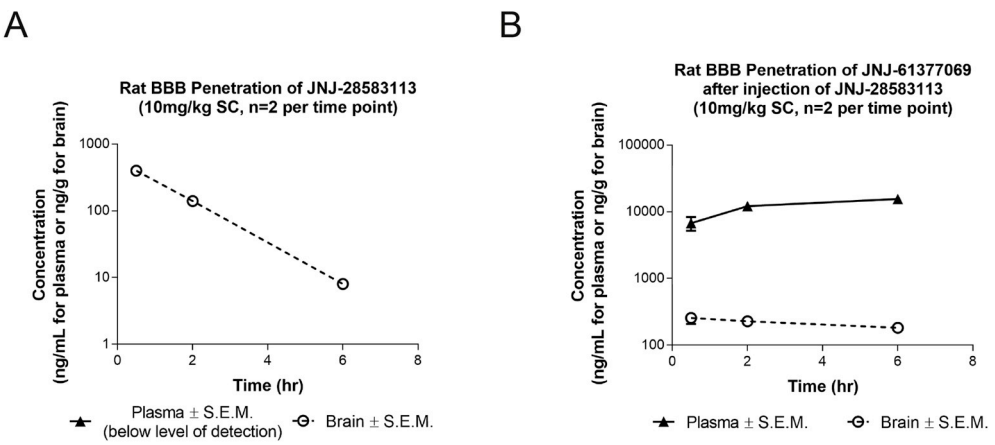

Fig. 5. Pharmacokinetic of JNJ-28583113. (A) Analysis of JNJ-28583113 levels in plasma and brain samples from rat dosed with JNJ-28583113 (10 mg/kg s.c.) showing that JNJ-28583113 is brain penetrant and achieved 400 ng/ml in the brain compartment. (B) Analysis of JNJ-61377069 levels in plasma and brain samples from rat dosed with JNJ-28583113 (10 mg/kg s.c.). Symbols represent mean ± S.E.M for plasma and brain samples collected from 2 different animals per time point.

drug-like molecules with better oral bioavailability and in-vivo pharmacodynamic efficacy compared to JNJ-28583113.

To address potential cross reactivity of the compound, we profiled JNJ-28583113 against most common kinases, GPCRs, ion channels and nine other TRP channels (based on commercial availabilities). Overall, JNJ-28583113 did not show any significant cross-reactivity in the assays performed except against TRPM5. TRPM5 is expressed in taste cells, gastrointestinal tract, pancreas and brainstem and current TRPM5 inhibitors display low potency and most of them cross react with TRPM4 (Liman, 2014). Therefore JNJ-28583113 could also be a good tool to assess TRPM5 functions although we have not yet further explored the effect of JNJ-28583113 on TRPM5 mediated signaling. Although TRPM2 and TRPM5 present little overlap in their expression pattern, one still needs to keep in mind potential confounding phenotypes while using JNJ-28583113 in cells or tissue that express both TRPM2 and TRPM5 such as pancreatic cells (Colsoul et al., 2013). None of the cells used in this manuscript express TRPM5. Finally, some TRP channels have be shown to form hetero-tetramers (Broker-Lai et al., 2017; Hoenderop et al., 2003). To date, cryo-EM studies have shown that TRPM2 forms homo-tetramers but additional structure function studies would be needed to understand its conformation in native systems as it could impact drug properties (Maruyama et al., 2007; Zhang et al., 2018b).

Previous studies have shown that there is an association between TRPM2 gene and bipolar disorder (BD) (McQuillin et al., 2006; Xu et al., 2009). In addition, TRPM2 deficient animals (TRPM2$^{-/-}$) present increased phosphorylation of inhibitory serine residues on GSK-3α and GSK-3β leading to decreased GSK-3 mediated signaling (Jang et al., 2015; Xie et al., 2011). One of Lithium's effect, the standard of care for patients with BD, is to reduce GSK-3 signaling by increasing phosphorylation of inhibitory residues (Alda, 2015). Therefore, Lithium had no effects in TRPM2$^{-/-}$ animals as basal level of phosphorylation of GSK-3 inhibitory residues were already at ceiling in those animals. When applying H_2O_2 on cells expressing hTRPM2, we induced a robust de-phosphorylation of GSK-3α and GSK-3β inhibitory residues that was reversed by JNJ-28583113 showing that inhibiting TRPM2 mimicked Lithium's effect on GSK-3 mediated signaling. Further experiments will be needed to explore if TRPM2 antagonists and Lithium have synergistic or parallel actions onto GSK-3 mediated signaling. GSK-3 is a central enzyme at the intersection of many signaling pathways and GSK-3 meditated signaling has been shown to be deregulated in multiple neurodegenerative and neuropsychiatric disorders (Beurel et al., 2015). Therefore, the use of TRMP2 antagonists might be a novel way to affect this key cellular player. Unfortunately, JNJ-28583113 is less than an ideal compound to test this hypothesis *in-vivo* in efficacy studies. We remain optimistic that the further development of a TRPM2 antagonist with better brain pharmacokinetic properties may help us observe similar Lithium-like phenotypes in an *in-vivo* model of cellular stress.

In addition, we showed that JNJ-28583113 protected cells from oxidative stress induced cell death, oxidative stress induced cellular morphological changes and blunted microglia cytokine release in response to pro-inflammatory stimuli. Oxidative stress and inflammation, are frequently observed in many disorders including Alzheimer's disease (AD). One of the hallmark of AD is the presence of increasing amounts of β-amyloid oligomers (βAOs) in patient's brain over the course of the disease. A recent publication showed that βAOs increase TRPM2 mediated signaling in neurons. Moreover, an animal model of AD also deficient in TRPM2 protein expression (APP/PS1/TRPM2$^{-/-}$) shows reduced synaptic loss, reduced microglia activation and improved cognition (Ostapchenko et al., 2015). It was also recently shown that TRPM2 deficient microglia present decreased cytokine release in response to βAOs (Alawieyah Syed Mortadza et al., 2018). These finding suggest that therapeutically targeting TRPM2 mediated signaling could improve the outcome of AD and highlight the need for TRPM2 antagonists with drug like properties.

In summary, this study contributes to the following in the TRPM2 field: (1) describes a potent reversible TRPM2 antagonist; (2) the first brain-penetrant TRPM2 antagonist, although the brain pharmacokinetic properties remain to be optimized with the next generation of compounds; (3) lays the foundation of more medicinal chemistry and discovery work to elucidate the role of TRPM2 in CNS pathophysiology.

Conflicts of interest

The authors declare no competing interests.

Acknowledgements:

We would like to thank Louis-Philippe Bernier and Brian MacVicar for their help in characterizing JNJ-28583113 (Centre for Brain Health, University of British Columbia, Vancouver, BC V6T 1Z4, Canada)

References

Alawieyah Syed Mortadza, S., Sim, J.A., Neubrand, V.E., Jiang, L.H., 2018. A critical role of TRPM2 channel in Abeta42 -induced microglial activation and generation of tumor necrosis factor-alpha. Glia 66, 562–575.
Alda, M., 2015. Lithium in the treatment of bipolar disorder: pharmacology and pharmacogenetics. Mol. Psychiatr. 20, 661–670.
Aminzadeh, M., Roghani, M., Sarfallah, A., Riazi, G.H., 2018. TRPM2 dependence of ROS-induced NLRP3 activation in Alzheimer's disease. Int. Immunopharmacol. 54, 78–85.
Beurel, E., Grieco, S.F., Jope, R.S., 2015. Glycogen synthase kinase-3 (GSK3): regulation, actions, and diseases. Pharmacol. Ther. 148, 114–131.
Broker-Lai, J., Kollewe, A., Schindeldecker, B., Pohle, J., Nguyen Chi, V., Mathar, I., Guzman, R., Schwarz, Y., Lai, A., Weissgerber, P., Schwegler, H., Dietrich, A., Both, M., Sprengel, R., Draguhn, A., Kohr, G., Fakler, B., Flockerzi, V., Bruns, D., Freichel, M., 2017. Heteromeric channels formed by TRPC1, TRPC4 and TRPC5 define hippocampal synaptic transmission and working memory. EMBO J. 36, 2770–2789.
Chen, G.L., Zeng, B., Eastmond, S., Elsenussi, S.E., Boa, A.N., Xu, S.Z., 2012.

Pharmacological comparison of novel synthetic fenamate analogues with econazole and 2-APB on the inhibition of TRPM2 channels. Br. J. Pharmacol 167, 1232–1243.
Colsoul, B., Nilius, B., Vennekens, R., 2013. Transient receptor potential (TRP) cation channels in diabetes. Curr. Top. Med. Chem. 13, 258–269.
Faouzi, M., Penner, R., 2014. Trpm2. Handb. Exp. Pharmacol. 222, 403–426.
Fonfria, E., Marshall, I.C., Boyfield, I., Skaper, S.D., Hughes, J.P., Owen, D.E., Zhang, W., Miller, B.A., Benham, C.D., McNulty, S., 2005. Amyloid beta-peptide(1-42) and hydrogen peroxide-induced toxicity are mediated by TRPM2 in rat primary striatal cultures. J. Neurochem. 95, 715–723.
Gustafsdottir, S.M., Ljosa, V., Sokolnicki, K.L., Anthony Wilson, J., Walpita, D., Kemp, M.M., Petri Seiler, K., Carrel, H.A., Golub, T.R., Schreiber, S.L., Clemons, P.A., Carpenter, A.E., Shamji, A.F., 2013. Multiplex cytological profiling assay to measure diverse cellular states. PLoS One 8, e80999.
Hara, Y., Wakamori, M., Ishii, M., Maeno, E., Nishida, M., Yoshida, T., Yamada, H., Shimizu, S., Mori, E., Kudoh, J., Shimizu, N., Kurose, H., Okada, Y., Imoto, K., Mori, Y., 2002. LTRPC2 Ca2+-permeable channel activated by changes in redox status confers susceptibility to cell death. Mol. Cell 9, 163–173.
Hill, K., Benham, C.D., McNulty, S., Randall, A.D., 2004a. Flufenamic acid is a pH-dependent antagonist of TRPM2 channels. Neuropharmacology 47, 450–460.
Hill, K., McNulty, S., Randall, A.D., 2004b. Inhibition of TRPM2 channels by the antifungal agents clotrimazole and econazole. Naunyn-Schmiedeberg's archives of pharmacology 370, 227–237.
Hoenderop, J.G., Voets, T., Hoefs, S., Weidema, F., Prenen, J., Nilius, B., Bindels, R.J., 2003. Homo- and heterotetrameric architecture of the epithelial Ca2+ channels TRPV5 and TRPV6. EMBO J. 22, 776–785.
Jang, Y., Lee, S.H., Lee, B., Jung, S., Khalid, A., Uchida, K., Tominaga, M., Jeon, D., Oh, U., 2015. TRPM2, a susceptibility gene for bipolar disorder, regulates glycogen synthase kinase-3 activity in the brain. J. Neurosci. : the official journal of the Society for Neuroscience 35, 11811–11823.
Kaufman, R.J., 1999. Stress signaling from the lumen of the endoplasmic reticulum: coordination of gene transcriptional and translational controls. Genes Dev. 13, 1211–1233.
Knowles, H., Li, Y., Perraud, A.L., 2013. The TRPM2 ion channel, an oxidative stress and metabolic sensor regulating innate immunity and inflammation. Immunol. Res. 55, 241–248.
Ko, S.Y., Wang, S.E., Lee, H.K., Jo, S., Han, J., Lee, S.H., Choi, M., Jo, H.R., Seo, J.Y., Jung, S.J., Son, H., 2019. Transient receptor potential melastatin 2 governs stress-induced depressive-like behaviors. Proc. Natl. Acad. Sci. U.S.A. 116, 1770–1775.
Kraft, R., Grimm, C., Frenzel, H., Harteneck, C., 2006. Inhibition of TRPM2 cation channels by N-(p-amylcinnamoyl)anthranilic acid. Br. J. Pharmacol 148, 264–273.
Kraft, R., Grimm, C., Grosse, K., Hoffmann, A., Sauerbruch, S., Kettenmann, H., Schultz, G., Harteneck, C., 2004. Hydrogen peroxide and ADP-ribose induce TRPM2-mediated calcium influx and cation currents in microglia. Am. J. Physiol. Cell Physiol. 286, C129–C137.
Lange, I., Yamamoto, S., Partida-Sanchez, S., Mori, Y., Fleig, A., Penner, R., 2009. TRPM2 functions as a lysosomal Ca2+-release channel in beta cells. Sci. Signal. 2, ra23.
Li, F., Abuarab, N., Sivaprasadarao, A., 2016. Reciprocal regulation of actin cytoskeleton remodelling and cell migration by Ca2+ and Zn2+: role of TRPM2 channels. J. Cell Sci. 129, 2016–2029.
Li, N., Ragheb, K., Lawler, G., Sturgis, J., Rajwa, B., Melendez, J.A., Robinson, J.P., 2003. Mitochondrial complex I inhibitor rotenone induces apoptosis through enhancing mitochondrial reactive oxygen species production. J. Biol. Chem. 278, 8516–8525.
Li, X., Jiang, L.H., 2018. Multiple molecular mechanisms form a positive feedback loop driving amyloid beta42 peptide-induced neurotoxicity via activation of the TRPM2 channel in hippocampal neurons. Cell Death Dis. 9, 195.
Liman, E.R., 2014. Trpm5. Handb. Exp. Pharmacol. 222, 489–502.
Luo, X., Li, M., Zhan, K., Yang, W., Zhang, L., Wang, K., Yu, P., Zhang, L., 2018. Selective inhibition of TRPM2 channel by two novel synthesized ADPR analogues. Chem. Biol. Drug Des 91, 552–566.
Maruyama, Y., Ogura, T., Mio, K., Kiyonaka, S., Kato, K., Mori, Y., Sato, C., 2007. Three-dimensional reconstruction using transmission electron microscopy reveals a swollen, bell-shaped structure of transient receptor potential melastatin type 2 cation channel. J. Biol. Chem. 282, 36961–36970.
McHugh, D., Flemming, R., Xu, S.Z., Perraud, A.L., Beech, D.J., 2003. Critical intracellular Ca2+ dependence of transient receptor potential melastatin 2 (TRPM2) cation channel activation. J. Biol. Chem. 278, 11002–11006.
McQuillin, A., Bass, N.J., Kalsi, G., Lawrence, J., Puri, V., Choudhury, K., Detera-Wadleigh, S.D., Curtis, D., Gurling, H.M., 2006. Fine mapping of a susceptibility locus for bipolar and genetically related unipolar affective disorders, to a region containing the C21ORF29 and TRPM2 genes on chromosome 21q22.3. Mol. Psychiatr. 11, 134–142.
Miyanohara, J., Kakae, M., Nagayasu, K., Nakagawa, T., Mori, Y., Arai, K., Shirakawa, H., Kaneko, S., 2018. TRPM2 channel aggravates CNS inflammation and cognitive impairment via activation of microglia in chronic cerebral hypoperfusion. J. Neurosci. Off. J. Soc. Neurosci. 38, 3520–3533.
Ostapchenko, V.G., Chen, M., Guzman, M.S., Xie, Y.F., Lavine, N., Fan, J., Beraldo, F.H., Martyn, A.C., Belrose, J.C., Mori, Y., MacDonald, J.F., Prado, V.F., Prado, M.A., Jackson, M.F., 2015. The transient receptor potential melastatin 2 (TRPM2) channel contributes to beta-amyloid oligomer-related neurotoxicity and memory impairment. J. Neurosci. Off. J. Soc. Neurosci. 35, 15157–15169.
Perraud, A.L., Schmitz, C., Scharenberg, A.M., 2003. TRPM2 Ca2+ permeable cation channels: from gene to biological function. Cell Calcium 33, 519–531.
Perraud, A.L., Takanishi, C.L., Shen, B., Kang, S., Smith, M.K., Schmitz, C., Knowles, H.M., Ferraris, D., Li, W., Zhang, J., Stoddard, B.L., Scharenberg, A.M., 2005. Accumulation of free ADP-ribose from mitochondria mediates oxidative stress-induced gating of TRPM2 cation channels. J. Biol. Chem. 280, 6138–6148.
Rudakova, E.V., Boltneva, N.P., Makhaeva, G.F., 2011. Comparative analysis of esterase activities of human, mouse, and rat blood. Bull. Exp. Biol. Med. 152, 73–75.
Song, K., Wang, H., Kamm, G.B., Pohle, J., Reis, F.C., Heppenstall, P., Wende, H., Siemens, J., 2016. The TRPM2 channel is a hypothalamic heat sensor that limits fever and can drive hypothermia. Science 353, 1393–1398.
Starkus, J., Beck, A., Fleig, A., Penner, R., 2007. Regulation of TRPM2 by extra- and intracellular calcium. J. Gen. Physiol. 130, 427–440.
Starkus, J.G., Poerzgen, P., Layugan, K., Kawabata, K.G., Goto, J.I., Suzuki, S., Myers, G., Kelly, M., Penner, R., Fleig, A., Horgen, F.D., 2017. Scalaradial is a potent inhibitor of transient receptor potential melastatin 2 (TRPM2) ion channels. J. Nat. Prod. 80, 2741–2750.
Sumoza-Toledo, A., Penner, R., 2011. TRPM2: a multifunctional ion channel for calcium signalling. J. Physiol. 589, 1515–1525.
Syed Mortadza, S.A., Wang, L., Li, D., Jiang, L.H., 2015. TRPM2 channel-mediated ROS-sensitive Ca(2+) signaling mechanisms in immune cells. Front. Immunol. 6, 407.
Takahashi, N., Kozai, D., Kobayashi, R., Ebert, M., Mori, Y., 2011. Roles of TRPM2 in oxidative stress. Cell Calcium 50, 279–287.
Tan, C.H., McNaughton, P.A., 2016. The TRPM2 ion channel is required for sensitivity to warmth. Nature 536, 460–463.
Togashi, K., Inada, H., Tominaga, M., 2008. Inhibition of the transient receptor potential cation channel TRPM2 by 2-aminoethoxydiphenyl borate (2-APB). Br. J. Pharmacol 153, 1324–1330.
Wehrhahn, J., Kraft, R., Harteneck, C., Hauschildt, S., 2010. Transient receptor potential melastatin 2 is required for lipopolysaccharide-induced cytokine production in human monocytes. J. Immunol. 184, 2386–2393.
Xie, Y.F., Belrose, J.C., Lei, G., Tymianski, M., Mori, Y., Macdonald, J.F., Jackson, M.F., 2011. Dependence of NMDA/GSK-3beta mediated metaplasticity on TRPM2 channels at hippocampal CA3-CA1 synapses. Mol. Brain 4, 44.
Xu, C., Li, P.P., Cooke, R.G., Parikh, S.V., Wang, K., Kennedy, J.L., Warsh, J.J., 2009. TRPM2 variants and bipolar disorder risk: confirmation in a family-based association study. Bipolar Disord. 11, 1–10.
Yamamoto, S., Shimizu, S., Kiyonaka, S., Takahashi, N., Wajima, T., Hara, Y., Negoro, T., Hiroi, T., Kiuchi, Y., Okada, T., Kaneko, S., Lange, I., Fleig, A., Penner, R., Nishi, M., Takeshima, H., Mori, Y., 2008. TRPM2-mediated Ca2+influx induces chemokine production in monocytes that aggravates inflammatory neutrophil infiltration. Nat. Med. 14, 738–747.
Zhang, H., Liu, H., Luo, X., Wang, Y., Liu, Y., Jin, H., Liu, Z., Yang, W., Yu, P., Zhang, L., Zhang, L., 2018a. Design, synthesis and biological activities of 2,3-dihydroquinazolin-4(1H)-one derivatives as TRPM2 inhibitors. Eur. J. Med. Chem. 152, 235–252.
Zhang, W., Chu, X., Tong, Q., Cheung, J.Y., Conrad, K., Masker, K., Miller, B.A., 2003. A novel TRPM2 isoform inhibits calcium influx and susceptibility to cell death. J. Biol. Chem. 278, 16222–16229.
Zhang, Z., Toth, B., Szollosi, A., Chen, J., Csanady, L., 2018b. Structure of a TRPM2 channel in complex with Ca(2+) explains unique gating regulation. Elife 7.
Zhong, Z., Zhai, Y., Liang, S., Mori, Y., Han, R., Sutterwala, F.S., Qiao, L., 2013. TRPM2 links oxidative stress to NLRP3 inflammasome activation. Nat. Commun. 4, 1611.